Published in final edited form as:
Clin Experiment Ophthalmol. 2009 January ; 37(1): 54–67. doi:10.1111/j.1442-9071.2008.01892.x.

High-resolution ultrasound imaging of the eye – a review

Ronald H Silverman, PhD
Weill Cornell Medical College and Riverside Research Institute, New York, USA

Abstract

This report summarizes the physics, technology and clinical application of ultrasound biomicroscopy (UBM) of the eye, in which frequencies of 35 MHz and above provide over a threefold improvement in resolution compared with conventional ophthalmic ultrasound systems. UBM allows imaging of anatomy and pathology involving the anterior segment, including regions obscured by overlying optically opaque anatomic or pathologic structures. UBM provides diagnostically significant information in conditions such as glaucoma, cysts and neoplasms, trauma and foreign bodies. UBM also can provide crucial biometric information regarding anterior segment structures, including the cornea and its constituent layers and the anterior and posterior chambers. Although UBM has now been in use for over 15 years, new technologies, including transducer arrays, pulse encoding and combination of ultrasound with light, offer the potential for significant advances in high-resolution diagnostic imaging of the eye.

Keywords

anterior segment; imaging; eye; ultrasound biomicroscopy

Introduction

The ideal diagnostic imaging device would allow non-invasive visualization of occult structures with infinite detail and perfect contrast in real time. It would also be easy to use and inexpensive. The superficial location of the eye and its cystic structure in combination with the presence of optical windows (the cornea and pupil) has rendered the eye a virtual test-bed for new imaging technologies including optical coherence tomography (OCT), magnetic resonance imaging (MRI), scanning Scheimpflug and slit-lamp devices and ultrasound.

In respect to the above criteria, MRI provides high contrast and good resolution, but is expensive, inconvenient and slow. Optical methods can provide excellent resolution, are cost-effective and easy to use, but are susceptible to intervening optically opaque structures, including normal anatomy (sclera, iris) and pathology (haemorrhage, corneal scars, cataract).

Ultrasound provides real-time cross-sectional images in a very cost-effective manner, even in the presence of optically opaque intervening structures. The use of ultrasound for diagnostic imaging of the eye originates with the work of Mundt and Hughes[1] (A-scan) and Baum and Greenwood[2] (B-scan) in the 1950s. Although there have been huge improvements in scanning, data processing and display technologies since then, the centre frequency of ophthalmic ultrasound units has almost, since the inception of the technology, remained at or near 10 MHz.

Correspondence: Dr Ronald Silverman, Department of Ophthalmology, Weill Cornell Medical College, 1300 York Avenue, Room LC304, New York, NY 10021, USA. ros2012@med.cornell.edu.

Disclosure: The author has a financial interest in ArcScan, Inc.

Although certainly useful for assessment of many ocular pathologies, the resolution obtainable at 10 MHz is over an order of magnitude poorer than that of OCT.

Ultrasound biomicroscopy (UBM) involves use of much higher frequencies (35–50 MHz) than those used in conventional ophthalmic B-scanners. The resulting improvement in resolution to 40 mm or less brings ultrasound closer to meeting the criteria for the ideal imaging device.

This paper will describe the physical basis, technical development and clinical applications of UBM.

The physics of ultrasound

A basic understanding of the physical principles and technology of ultrasound is required to fully appreciate the clinical capabilities and limitations of UBM.

Ultrasound consists of waves of compression and rarefaction propagating through a medium. Wavelength and frequency are defined by the relation $c = \upsilon\lambda$, where c is the speed-of-sound, λ is wavelength, and υ is frequency. The speed-of-sound is related to the medium's composition and temperature, but is largely independent of frequency. Acoustic reflection occurs at interfaces between regions of different acoustic impedance (density × speed-of-sound). Scattering occurs where these discontinuities are smaller than a wavelength. Attenuation of ultrasound occurs as it propagates through tissues as a consequence of reflection, scattering and absorption. Attenuation increases exponentially with both tissue depth and frequency.

The ultrasound probe contains a piezoelectric material, the transducer, which expands or contracts when an electrical voltage is placed across it. This is communicated to the fluid with which the transducer is in contact. Ultrasound may be focused by placing an acoustic lens over the surface of a flat transducer or by forming the piezoelectric material into a curved surface of suitable radius. After emitting an acoustic pulse, the transducer waits passively for echoes to return before it emits another pulse. Echoes interact with the piezoelectric element and the resulting voltages are then amplified and processed to form images and perform biometry. The range to a reflector can be computed from the speed-of-sound, c, and the time interval, t, between pulse emission and echo return, specifically, range = $ct/2$. Two-dimensional images, referred to as *B-scans*, are generated by mechanically scanning the transducer and setting pixel intensity in proportion to echo amplitude along each line-of-sight.

Axial resolution refers to how close together two reflectors can be along the direction of acoustic propagation while still being distinguishable from each other. Axial resolution is computed as $cT/2$, where T is pulse duration. Lateral resolution refers to the ultrasound system's ability to distinguish two reflectors positioned next to each other with respect to the ultrasound beam axis. This is affected by both transducer frequency and focal properties, specifically focal length, L, and aperture, D. The ratio of these two properties defines f, the transducer's f-number. Lateral resolution in the focal plane is computed as $L\lambda/D$ or $f\lambda$. As the f-ratio decreases, the transducer becomes more highly focused and lateral resolution improves, but the region along the beam axis in which the transducer is well focused, the *depth-of-field*, becomes progressively smaller.

The piezoelectric element of conventional 10 MHz transducers is most often a ceramic material, lead zirconate (PZT). Use of PZT for frequencies above 15–20 MHz is impracticable because the brittle PZT crystal cannot be made thin enough to generate higher frequencies without cracking. Consequently, UBM devices could not be fabricated until an alternative material became available. Polyvinylidene fluoride (PVDF) is a piezopolymer that, unlike PZT, is highly flexible and readily available in thin sheets. A 9 mm thick PVDF membrane, for instance, can be used to form the piezoelectric element of a 50 MHz probe. Sherar and Foster

reported on the use of PVDF to fabricate a UBM transducer in 1989.[3] More recently, the co-polymer polyvinylidene fluoride trifluoroethylene (PVDF-TrFE) has largely replaced PVDF because of its greater sensitivity.[4]

The properties of a typical 10 MHz transducer that might be used for general-purpose ophthalmic imaging and a 50 MHz transducer of the type typical for UBM systems are compared in Table 1. Note the far smaller depth-of-field of the UBM probe, which is under 1 mm, compared with the 10 MHz ophthalmic probe. Also note that whereas attenuation in water is negligible at 10 MHz, this is a significant effect at 50 MHz – the signal at the centre frequency would be reduced by over 13 dB after propagating 12 mm to the focus and back.

UBM systems

The first practical UBM system for imaging of the eye was developed by Foster and Pavlin in the early 1990s.[5,6] The ultrasound biomicroscope, manufactured by Zeiss-Humphrey Instruments (San Leandro, CA, USA), was an outgrowth of this work. This instrument allowed widespread access to UBM technology and clinical application. Coleman *et al.* independently developed a UBM system emphasizing the processing of raw radiofrequency echo data acquired in sequential planes suitable for 3-D analysis, especially corneal biometric analysis.[7] This system also was eventually commercialized as the Artemis-2 system by Ultralink, LLC (St Petersburg, FL, USA).

The Zeiss-Humphrey (later Paradigm Medical Industries, Salt Lake City, UT, USA) UBM consisted of a 50 MHz probe that was supported by an articulated arm. The transducer itself was not sealed within the probe as is typical for 10 MHz systems so as to avoid attenuation by the cap. The probe provided a scan rate of 8 Hz, giving real-time imaging, with scans consisting of 256 lines-of-sight (vectors) over a 5 mm × 5 mm field. This allowed imaging of anatomic areas of interest in the anterior segment, but not the whole anterior segment in a single scan. After topical anaesthesia, the probe was coupled to the eye using a scleral shell that held the eyelids open and filled with normal saline or the more viscous methycellulose for acoustic coupling.

The Ultralink Artemis-2 used an arc-scan mechanism to maintain normality between the ultrasound beam axis and the corneal surface to facilitate corneal biometric analysis and also provided sufficient scan width to visualize the anterior segment from sulcus to sulcus. It incorporated a fixation light and video camera to maintain and monitor eye position during scanning. The Artemis-2 is no longer produced, but the technology is currently being further developed by Arcscan, Inc. (Morrison, CO, USA).

Numerous manufacturers including Quantel Medical Instruments (Bozeman, MT, USA), Optikon (Rome, Italy), Sonomed (Lake Success, NY, USA) and Ophthalmic Technologies, (Toronto, ON, USA), among others, now make UBMs with higher scan rates and more compact handheld probes than that of the original Zeiss-Humphrey UBM. IScience (Menlo Park, CA, USA) manufactures an 80 MHz scanner for high-resolution imaging of the angle and Schlemm's canal. In some cases these instruments provide scan width sufficient to encompass the entire anterior segment.

Clinical application

Ultrasound biomicroscopy systems are suitable for imaging of virtually all anterior segment anatomy and pathology, including the cornea, iridocorneal angle, anterior chamber, iris, ciliary body and lens. UBM is thus applicable for diagnostic imaging of corneal diseases, glaucoma, cysts and tumours as well as lens implants. Although exams are most commonly performed with a fluid-filled scleral shell, they may also utilize a waterbath, a membrane enclosed-tip

applied to the eye after topical anaesthetic or even through closed lids, especially in cases of trauma, albeit at the cost of reduced sensitivity due to attenuation by the lids.

The appearance of a normal anterior segment on UBM is presented in Figure 1. This scan demonstrates all anterior segment structures, including the anterior lens surface, zonules and ciliary body.

The earliest clinical UBM studies, which were carried out by Pavlin *et al.*, examined the anterior segment in glaucoma.[8,9] Pavlin *et al.* showed the utility of UBM in characterizing several forms of glaucoma, including plateau iris syndrome[10] and pupillary block,[11] which together constitute the most common forms of primary angle closure glaucoma.[12] In pupillary block (Fig. 2, top), pressure in the posterior chamber is elevated relative to that of the anterior chamber owing to impairment of the flow of aqueous through the pupil. This results in forward bowing of the iris from the root to the pupil margin in the presence of a formed posterior chamber. Laser iridotomy will result in iris flattening by relieving the anterior/posterior chamber pressure differential. In plateau iris syndrome, the ciliary body is anteriorly positioned and possibly enlarged, compressing the iridocorneal angle and impairing outflow. UBM will demonstrate little bowing, but rather anterior positioning of the ciliary body and closing of the sulcus. In plateau iris syndrome, the UBM plays an invaluable role by allowing demonstration of anterior displacement of the ciliary processes and sulcus closure (Fig. 2, bottom). UBM can also be useful for diagnostic imaging of malignant glaucoma, which is characterized by a flattened anterior chamber, typically following glaucoma surgery, chronic angle closure glaucoma or pseudoexfoliation.[13] UBM has also been shown to be of value in elucidating the aetiology of pseudophakic pupillary block glaucoma.[14,15] The UBM appearance of pigment dispersion glaucoma, a condition characterized by loss of pigment from the posterior iris surface with consequent impairment of trabecular outflow, was first described by Pavlin *et al.*[16] Pigment dispersion glaucoma often demonstrates iris concavity, consistent with the hypothesis that iris-lens chafing is responsible for dispersion of pigment particles. UBM is a useful tool in guidance and evaluation in glaucoma surgery,[17] including evaluation of the bleb and Schlemm's canal in procedures such as deep sclerectomy and canaloplasty.[18,19] An example of an 80 MHz scan of the angle is provided in Figure 3.

In 1992, Pavlin *et al.* described biometric criteria that could be used for reproducible measurement of various anterior segment structures.[8] These included the angle opening at 250 and 500 μm from the scleral spur, scleral thickness at the spur, trabecular-ciliary process distance, iris thickness at specific positions, among others. Ishikawa, Liebman and Ritch described further criteria in 2000, especially numeric descriptors of angle geometry.[20] These criteria are of importance in allowing definition of reproducible criteria for characterizing different glaucoma types. Marchini,[21,22] for instance, used UBM to biometrically compare different forms of angle closure glaucoma, and Sihota *et al.*[23] applied these criteria for comparing subtypes of primary angle closure glaucoma.

Ultrasound biomicroscopy allows assessment of primary and secondary cysts of the anterior segment.[24–26] Primary neuroepithelial cysts involve the pigment epithelium of the iris and ciliary body, and may thus appear anywhere along the posterior iris surface through the pars plana, although the iridociliary junction is most common. Primary cysts generally appear with thin, rounded reflective walls with sonolucent, fluid-filled interiors (Fig. 4). Multiple cysts are not unusual. Large cysts in the region of the sulcus may cause the iris to bulge and narrow or close the angle. Although primary cysts may be associated with underlying disease such as uveitis,[27] they are common in normal asymptomatic eyes as well.[28] Secondary implantation cysts may arise as a result of penetrating trauma or ocular surgery due to deposition of epithelial cells from the eyelid, cornea or conjunctiva on the iris. Implantation cysts may appear in the

anterior chamber and often display diffuse or dense internal echoes. Finally, cysts may also be associated with neoplasms, including malignant melanoma and medulloepithelioma.[29–31]

Malignant melanomas (Fig. 5) may occur in either the iris or ciliary body, but their prognoses are quite different. Ciliary body involvement is associated with high risk of metastatic spread and mortality. Melanomas solely involving the iris tend to be indolent and rarely metastasize, although risk may increase as a consequence of invasive procedures including glaucoma surgery.[31] In patients presenting with a pigmented lesion in the angle, UBM can show if the lesion is restricted to the iris or extends into the ciliary body. Tumours involving the ciliary body may cause iris bulging similar to that caused by retroiridal cysts, and UBM can play a crucial role in differentiating the one from the other. Assessment of neoplasms such as malignant melanoma by UBM allows precise localization in relation to anterior segment structures and determination of tumour thickness and width for planning of brachytherapy. UBM offers a valuable and non-invasive means to assess tissue characteristics, growth and invasion of adjacent structures. UBM also allows assessment of conjunctival masses, including intraocular extension (Fig. 6).

Pavlin *et al.* first described the use of UBM for imaging of anterior segment tumours in the early 1990s.[32] Several subsequent studies have confirmed the value of UBM in documenting tumour progression, extension and regression, in many instances with histopathologic correlation.[33–36] Although there is considerable variation in the appearance of ciliary body melanomas on UBM, they typically exhibit a hemispherical shape with a homogeneous internal echo pattern of low to moderate reflectivity. Cystic spaces, however, are not uncommon. UBM allows tumours to be characterized in terms of their thickness and width, which can be used to document growth or regression following treatment on follow-up exam. Although malignant melanoma of the eye is rare, other rare neoplasms may affect the anterior segment as well. UBM can play a role in differentiation of melanoma from adenoma,[37] medulloepithelioma[27] and melanocytoma.[38]

Pavlin *et al.* was the first to describe UBM imaging of the cornea.[6] The use of UBM as a diagnostic tool has been described for corneal pathologies including oedema,[39] keratoconus,[40,41] dystrophies,[42] corneal scars,[43,44] trauma[45] and for keloid.[46] Figure 7 shows how UBM can be used to measure scar depth, which may be a significant factor in patient management (e.g. penetrating *vs*. non-penetrating keratoplasty) and candidate selection in refractive corneal surgery.

Although measurement of central corneal thickness has long been performed with by use of contact ultrasound pachymeters operating at 20–50 MHz, UBM has the advantage of allowing imaging and biometry of 2-D corneal cross sections instead of at individual positions. Tam and Rothman[47] reported UBM and contact ultrasound pachymetry to give similar results in measurement of central corneal thickness, although our own recent findings comparing Artemis-2 and contact pachymetry showed the non-contact immersion method to give significantly thinner results than contact pachymetry.[48,49] This suggests that decentration or oblique incidence in contact pachymetry may cause spuriously thicker measurements.

The use of ultrasound for assessment of the cornea following excimer laser photokeratectomy was described by Allemann *et al.*[44] and Pavlin *et al.*[50] and their respective coworkers in the early 1990s. Allemann *et al.* used the prototype system developed by Coleman *et al.* that allowed acquisition of raw radiofrequency data and utilized calibrated backscatter spectroscopy to quantify scar density. Using the same device, Reinstein *et al.* demonstrated that UBM could resolve the epithelial surface from Bowman's membrane and described a signal-processing approach that allowed reproducible measurement of corneal and epithelial thickness.[51,52] Reinstein and Silver-man subsequently demonstrated that pachymetric maps

representing the thickness of corneal layers could be produced from a series of sequential, parallel scan planes of the central cornea.[53] However, the curved and highly specular surface of the cornea prevented acquisition of useful data outside the central 3 mm zone. This problem was overcome by development of an arc-scanner, which allowed the acoustic beam axis to maintain normality to the corneal surface while at the same time keeping the cornea within the focal zone.[54] Reinstein *et al.* used this system to image the full width of the cornea following laser *in situ* keratomileusis and demonstrated visualization of the flap (Fig. 8), measurement of residual stromal thickness and epithelial compensation for curvature changes induced by ablation of underlying stromal tissue.[55] Reinstein *et al.* recently reported preliminary results suggesting that the epithelium undergoes characteristic changes in its thickness distribution in keratoconus in response to subclinical bulging of the underlying stroma, and suggests that this may be useful in screening.[56] Examples of a layered corneal pachymetric maps following laser *in situ* keratomileusis and in keratoconus are provided in Figures 9 and 10.

Ultrasound biomicroscopy is generally useful for assessment of unexplained hypotony,[57,58] including the presence of cyclitic membranes[59] and traumatic cyclodialysis clefts.[60] UBM can be used as an effective diagnostic tool in cases of ocular trauma.[61,62] In cases of closed or open-globe trauma, UBM can be performed with topical anaesthesia. In some cases, the exam may be performed through closed lids. With an open globe care must be taken not to exert undo pressure on the globe and sterile media should be used. UBM can demonstrate iridodialysis, rupture of the anterior lens capsule, lens displacement, cyclodialysis, zonular defects, angle recession, intraocular foreign bodies in the presence of corneal scarring, hyphema (Fig. 11), cataract and lens subluxation (Fig. 12) and ciliary body detachment (Fig. 13).

The ability of UBM to visualize the posterior chamber is useful for assessment of the position of the crystalline lens and lens implants, including phakic and piggyback implants, as demonstrated in Figure 14. The crystalline lens normally gives specular surface reflectivity with minimal internal echoes. Nuclear and cortical cataracts can be readily visualized on UBM as regions of elevated internal reflectivity. Following cataract surgery, UBM can detect retained nuclear fragments posterior to the iris plane.[63] Haptic position can be determined in situations where unexplained pain, bleeding or other complications occur following posterior chamber lens implantation.[64] The biometry of the anterior segment can be measured by UBM systems that encompass the entire anterior segment. This allows preoperative evaluation of the position of the sulcus plane before cataract surgery, facilitating estimation of postoperative intraocular lens position. With phakic refractive lens implants, UBM can similarly aid by preoperative determination of sulcus plane diameter at specific meridians, avoiding problems with over- or undersized implants.[65,66] White-to-white is an unreliable means for estimation of internal ocular dimensions.[67]

Ultrasound biomicroscopy allows evaluation of scleral abnormalities, as demonstrated in Figure 15. UBM also allows assessment of the eyelids, including normal anatomy[68] and neoplasms.[69,70] Evaluation of the extraocular muscles in strabismus surgery by UBM has also been reported.[71]

UBM and other anterior segment imaging technologies

Several technologies now exist for imaging of the anterior segment, including OCT (e.g. Visante, Carl Zeiss Meditec AG, Jena, Germany), scanning Scheimpflug (e.g. Pentacam, Oculus, Lynnwood, WA, USA), and scanning slit-lamp systems (e.g. Orbscan, Orbtek, Salt Lake City, UT, USA). Each method has its particular advantages and disadvantages in relation to each other and to UBM.[72] All of the above optically based systems are limited by the presence of optical opacities, either in the form of normal anatomy (iris, sclera) or pathology (hyphaema, pigmented lesions). Optical systems, however, require no fluid coupling to the eye, and are

thus easier to use. They also naturally lend themselves to alignment by provision of a fixation target and an optical image of the eye during scanning, which is not the case for ultrasound systems other than the Artemis. Optical systems also offer high-speed 3-D scanning of the anterior segment, facilitating biometric analysis of corneal thickness and anterior chamber dimensions.

The future

Current ophthalmic UBM systems use focused, single-element transducers because of the complexity and expense of fabrication of high-frequency array transducers. High-frequency annular arrays consisting of a few concentric piezoelectric rings are relatively easy to fabricate, however, and by use of synthetic focusing can greatly extend the depth-of-field compared with single-element probes.[73] Although annular arrays must still be mechanically scanned to obtain a 2-D image, this is not the case for high-frequency linear arrays now under development.[74] However, their lack of radial symmetry reduces lateral resolution in the elevation axis compared with that of an annular array. In the longer term, it is possible that 2-D high-frequency arrays based on micro-electromechanical systems constructed by chip fabrication techniques or other technologies may be realized. This would allow synthetic focusing, beam symmetry and electronic beam steering for nearly instantaneous 3-D imaging of the anterior segment. Examples of UBM images obtained with prototype annular and linear array UBM systems are shown in Fig. 16.

Current UBM systems use a short voltage impulse to excite the transducer. This is ideal for producing a highly damped acoustic pulse that maximizes axial resolution. However, this pulse strategy provides relatively low sensitivity, because only so much energy can be packed into such a pulse without exceeding ophthalmic safety guidelines for ultrasound exposure. An alternative is the use of pulse encoding in the form of a prolonged frequency-swept pulse train called a *chirp*. The maximum instantaneous intensity of the chirp is comparable to that of an impulse, but the duration is much longer. To recover the desired axial resolution, the echo data are digitally post-processed with a *compression filter*. This technique can improve signal-to-noise ratio by 20 dB or more, greatly increasing sensitivity and depth of penetration.[75]

Another field where potential advances are likely to occur is non-linear ultrasonic imaging, sometimes referred to as *tissue harmonic imaging*.[76] This modality is based on the progressive distortion an ultrasound wave undergoes as it propagates owing to the difference in the speed-of-sound between its compressed *versus* rarified components. Imaging at the second harmonic (2× the fundamental, emitted frequency) provides improved resolution compared with conventional imaging at the fundamental. Also, attenuation is reduced, as the harmonic need travel only in one direction. Special transducers have been demonstrated specifically for optimization of UBM harmonic imaging.[77]

High-frequency ultrasound blood flow imaging and measurement can be accomplished by either Doppler methods or a time-domain method called *swept mode*.[78] Although some concern exists regarding Doppler exposure levels, recent analysis suggests that high-frequency Doppler is safe for ophthalmic tissues.[79] A recent report also describes an intraoperative Doppler needle probe for measurement of flow in the retina and optic nerve.[80] Ultrasound contrast agents, usually gas-filled microbubbles, offer visualization of the microvasculature, including the targeting of specific biomolecules.[81]

Finally, we may see a merging of ultrasound with optics. Ultrasound can be used to increase OCT penetration via photon–phonon interaction.[82] It may also be possible to use the acoustic radiation force emitted by a transducer to ‘palpate’ thin ocular tissues such as the retina or cornea to image their elastic properties. This technique, called *acoustic radiation force imaging*,[83] is now used in non-ophthalmic clinical specialties, where tissue thicknesses are

measured in centimetres. The combination of acoustic radiation force imaging with the high resolution provided by OCT would allow very sensitive measurements of elasticity in the thin tissue layers of the eye. In *photoacoustic imaging*, optical pulses of a few nanoseconds duration cause thermoelastic expansion in tissues as a result of optical absorption, resulting in emission of broadband ultrasound signals that are detected by a UBM transducer acting only as a receiver. Such systems can thus produce simultaneous photoacoustic images of optical absorption and conventional pulse/echo UBM imaging.[84] Tuning of the light source wavelength allows photoacoustic imaging of specific molecules, such as haemoglobin (for imaging of microvasculature) or melanin (for the uvea and tumours),[85] although obviously compliance with ANSI standards for ophthalmic exposure must be taken into account.

Ultrasonic imaging of the eye has been undergoing progressive development for over a half century. It may thus be surprising that ultrasound technology is still undergoing rapid advances in many directions. Diagnostic imaging of the eye will be the beneficiary of these technologic innovations.

Acknowledgments

I would like to acknowledge the support of my mentors, D. Jackson Coleman, MD and the late Frederic L. Lizzi, EngScD. I would also like to thank my colleagues Vincenzina Mazzeo, MD, Roxana Ursea, MD, Dan Z. Reinstein, MD MA(Cantab) FRCSC and Norma Allemann, MD who contributed figures and advice, and Harriet Lloyd, MS, for her patience. Lastly, I would like to acknowledge the support of the Dyson Foundation and NIH grant EB000238.

References

1. Mundt GH, Hughes WF. Ultrasonics in ocular diagnosis. Am J Ophthalmol 1956;42:488–98. [PubMed: 13362453]
2. Baum G, Greenwood I. The application of ultrasonic locating techniques to ophthalmology. II. Ultrasonic slit-lamp in the ultrasonic visualization of soft tissues. Arch Ophthalmol 1958;60:263–79.
3. Sherar MD, Foster FST. The design and fabrication of high frequency poly(vinylide fluoride) transducers. Ultrason Imag 1989;11:75–94.
4. Foster FS, Harasiewicz KA, Sherar MD. A history of medical and biological imaging with polyvinylidene fluoride (PVDF) transducers. IEEE Trans Ultrason Ferroelectr Freq Control 2000;47:1363–71. [PubMed: 18238682]
5. Pavlin CJ, Sherar MD, Foster FS. Subsurface ultrasound microscopic imaging of the intact eye. Ophthalmology 1990;97:244–50. [PubMed: 2326015]
6. Pavlin CJ, Harasiewicz K, Sherar MD, Foster FS. Clinical use of ultrasound biomicroscopy. Ophthalmology 1991;98:287–95. [PubMed: 2023747]
7. Reinstein DZ, Silverman RH, Coleman DJ. High-frequency ultrasound measurement of the thickness of the corneal epithelium. Refract Corn Surg 1993;9:385–7.
8. Pavlin CJ, Harasiewicz K, Foster FS. Ultrasound biomicroscopy of anterior segment structures in normal and glaucomatous eyes. Am J Ophthalmol 1992;113:381–9. [PubMed: 1558111]
9. Pavlin CJ, Foster FS. Ultrasound biomicroscopy in glaucoma. Acta Ophthalmologica – Suppl 1992;204:7–9.
10. Pavlin CJ, Ritch R, Foster FS. Ultrasound biomicroscopy in plateau iris syndrome. Am J Ophthalmol 1992;113:390–95. [PubMed: 1558112]
11. Aslanides IM, Libre PE, Silverman RH, et al. High frequency ultrasound imaging in papillary block glaucoma. Br J Ophthalmol 1995;79:972–6. [PubMed: 8534666]
12. Mandell MA, Pavlin CJ, Weisbrod DJ, Simpson ER. Anterior chamber depth in plateau iris syndrome and papillary block as measured by ultrasound biomicroscopy. Am J Ophthalmol 2003;136:900–3. [PubMed: 14597043]
13. Trope GE, Pavlin CJ, Bau A, et al. Malignant glaucoma. Clinical ultrasound biomicroscopic features. Ophthalmology 1994;101:1030–5. [PubMed: 8008343]

14. Satish S, MacKinnon JR, Atta HR. Role of ultrasound biomicroscopy in managing pseudophakic pupillary block glaucoma. J Cataract Refract Surg 2000;26:1836–8. [PubMed: 11134889]
15. Kobayashi H, Hirose M, Kobayashi K. Ultrasound biomicroscopic analysis of pseudophakic pupillary block glaucoma induced by Soemmering's ring. Br J Ophthalmol 2000;84:1142–6. [PubMed: 11004100]
16. Pavlin CJ, Macken P, Trope GE, et al. Accommodation and iridotomy in the pigment dispersion syndrome. Ophthalmic Surg Lasers 1996;27:113–20. [PubMed: 8640433]
17. Yamamoto T, Sakuma T, Kitakawa Y. An ultrasound biomicroscopic study of filtering blebs after mitomycin C trabeculectomy. Ophthalmology 1995;102:1770–76. [PubMed: 9098276]
18. Khairy HA, Atta HR, Green FD, et al. Ultrasound biomicroscopy in deep sclerotomy. Eye 2005;19:555–60. [PubMed: 15761488]
19. Lewis RA, von Wolff K, Tetz M, et al. Canaloplasty: circumferential viscodilation and tensioning of Schlemm's canal using a flexible microcatheter for the treatment of open-angle glaucoma in adults: interim clinical study analysis. J Cataract Refract Surg 2007;33:1217–26. [PubMed: 17586378]
20. Ishikawa H, Liebmann JM, Ritch R. Quantitative assessment of the anterior segment using ultrasound biomicroscopy. Curr Opin Ophthalmol 2000;11:133–9. [PubMed: 10848220]
21. Marchini G. Biometric data and pathogenesis of angle closure glaucoma. Acta Ophth Scan 2002;80 (s236):13–14.
22. Marchini G, Pagliarusco A, Toscano A, et al. Ultrasound biomicroscopic and conventional ultrasonographic study of ocular dimensions in primary angle-closure glaucoma. Ophthalmology 1998;105:2091–8. [PubMed: 9818611]
23. Sihota R, Dada T, Gupta R, et al. Ultrasound biomicroscopy in the subtypes of primary angle closure glaucoma. J Glaucoma 2005;14:387–91. [PubMed: 16148588]
24. Marigo FA, Finger PT, McCormick SA, et al. Anterior segment implantation cysts. Ultrasound biomicroscopy with histopathologic correlation. Arch Ophthalmol 1998;116:1569–75. [PubMed: 9869783]
25. Marigo FA, Esaki K, Finger PT, et al. Differential diagnosis of anterior segment cysts by ultrasound biomicroscopy. Ophthalmology 1999;106:2131–5. [PubMed: 10571349]
26. Augsburger JJ, Affel LL, Benarosh DA. Ultrasound biomicroscopy of cystic lesions of the iris and ciliary body. Trans Am Ophthalmol Soc 1996;94:259–74. [PubMed: 8981700]
27. Gentile RC, Liebmann JM, Tello C, et al. Ciliary body enlargement and cyst formation in uveitis. Br J Ophthalmol 1996;80:895–9. [PubMed: 8976700]
28. Kunimatsu S, Araie M, Ohara K, Hamada C. Ultrasound biomicroscopy of ciliary body cysts. Am J Ophthalmol 1999;127:48–55. [PubMed: 9932998]
29. Zhou M, Xu G, Bojanowski CM, et al. Differential diagnosis of anterior chamber cysts with ultrasound biomicroscopy: ciliary body medulloepithelioma. Acta Ophthalmol Scan 2006;84:137–9.
30. Ayres B, Brasil OM, Klejnberg C, et al. Ciliary body medulloepithelioma: clinical ultrasound biomicroscopic and histopathologic correlation. Clin Exp Ophthalmol 2006;34:695–8.
31. Nordlund JR, Robertson DM, Herman DC. Ultrasound biomicroscopy in the management of malignant iris melanoma. Arch Ophthalmol 2003;121:725–7. [PubMed: 12742854]
32. Pavlin CJ, McWhae JA, McGowan HD, Foster FS. Ultrasound biomicroscopy of anterior segment tumors. Ophthalmology 1992;99:1220–8. [PubMed: 1513574]
33. Ursea R, Coleman DJ, Silverman RH, et al. Correlation of high-frequency ultrasound backscatter with tumor microstructure in iris melanoma. Ophthalmology 1998;105:906–12. [PubMed: 9593396]
34. Weisbrod DJ, Pavlin CJ, Emara K, et al. Small ciliary body tumors: ultrasound biomicroscopic assessment and follow-up of 42 patients. Am J Ophthalmol 2006;141:622–8. [PubMed: 16564795]
35. Conway RM, Chew T, Desai K, et al. Ultrasound biomicroscopy: role in diagnosis and management in 130 consecutive patients evaluated for anterior segment tumors. Br J Ophthalmol 2005;89:950–55. [PubMed: 16024841]
36. Torres VLL, Allemann N, Erwenne CM. Ultrasound biomicroscopy features of iris and ciliary body melanomas before and after brachytherapy. Ophthalmic Surg Lasers Imaging 2005;36:129–38. [PubMed: 15792314]

37. Shields JA, Shields CL, Mercado G, et al. Adenoma of the iris pigment epithelium: a report of 20 cases. Arch Ophthalmol 1999;117:736–41. [PubMed: 10369583]
38. Mohamed MD, Gupta M, Parsons A, Rennie IG. Ultrasound biomicroscopy in the management of melanocytoma of the ciliary body with extrascleral extension. Br J Ophthalmol 2005;89:14–16. [PubMed: 15615738]
39. Avitabile T, Russo V, Ghirlanda R, et al. Corneal oedemas: diagnosis and surgical planning with ultrasound biomicroscopy. Ophthalmologica 1998;212 (Suppl 1):13–16. [PubMed: 9730739]
40. Avitabile T, Marano F, Uva MG, Reibaldi A. Evaluation of central and peripheral corneal thickness with ultrasound biomicroscopy in normal and keratoconic eyes. Cornea 1997;16:639–44. [PubMed: 9395873]
41. Avitabile T, Franco L, Ortisi E, et al. Keratoconus staging. A computer-assisted ultrabiomicroscopic method compared with videokeratographic analysis. Cornea 2004;23:655–60. [PubMed: 15448489]
42. Rapuano CJ. Excimer laser phototherapeutic keratectomy in eyes with anterior corneal dystrophies: short-term clinical outcomes with and without an antihyperopia treatment and poor effectiveness of ultrasound biomicroscopic evaluation. Cornea 2005;24:20–31. [PubMed: 15604863]
43. Reinstein DZ, Aslanides IM, Silverman RH, et al. High-frequency ultrasound corneal pachymetry in the assessment of corneal scars for therapeutic planning. CLAO J 1994;20:198–203. [PubMed: 7955303]
44. Allemann N, Chamon W, Silverman RH, et al. High-frequency ultrasound quantitative analyses of corneal scarring following excimer laser keratectomy. Arch Ophthalmol 1993;111:968–73. [PubMed: 8328940]
45. Pavlin CJ, Foster FS. Ultrasound biomicroscopy. High-frequency ultrasound imaging of the eye at microscopic resolution. Rad Clin North Am 1998;36:1047–58.
46. Chawla B, Agarwal A, Kashyap S, Tandon R. Diagnosis and management of corneal keloid. Clin Exper Ophthalmol 2007;35:855–7.
47. Tam ES, Rootman DS. Comparison of central corneal thickness measurements by specular microscopy, ultrasound pachymetry, and ultrasound biomicroscopy. J Cataract Refract Surg 2003;29:1179–84. [PubMed: 12842687]
48. Greyrose SE, Starr CE, Lloyd HO, Silverman RH. Comparative central corneal thickness by ultrasound pachymetry, Artemis-2, and Visante. IOVS 2008;49 ARVO E-Abstract 1020.
49. Paul T, Lim M, Starr CE, Lloyd HO, Coleman DJ, Silverman RH. Central corneal thickness as measured by Orbscan II, ultrasound pachymeter and Artemis-2. J Cataract Refract Surg 2008;34:1906–12. [PubMed: 19006737]
50. Pavlin CJ, Harasiewicz K, Foster FS. Ultrasound biomicroscopic assessment of the cornea following excimer laser photokeratectomy. J Cataract Refract Surg 1994;20 (Suppl):206–11. [PubMed: 8006788]
51. Reinstein DZ, Silverman RH, Coleman DJ. High-frequency ultrasound measurement of the thickness of the corneal epithelium. Refract Corneal Surg 1993;9:385–7. [PubMed: 8241045]
52. Reinstein DZ, Silverman RH, Rondeau MJ, Coleman DJ. Epithelial and corneal thickness measurements by high-frequency ultrasound digital signal processing. Ophthalmology 1994;101:140–46. [PubMed: 8302547]
53. Reinstein DZ, Silverman RH, Trokel SL, Coleman DJ. Corneal pachymetric topography. Ophthalmology 1994;101:432–8. [PubMed: 8127563]
54. Silverman RH, Reinstein DZ, Raevsky T, Coleman DJ. Improved system for ultrasonic imaging and biometry. J Ultra Med 1997;16:117–24.
55. Reinstein DZ, Silverman RH, Coleman DJ. Very high-frequency ultrasound corneal analysis identifies anatomic correlates of optical complications of lamellar refractive surgery. Ophthalmology 1999;105:474–82. [PubMed: 10080202]
56. Reinstein, DZ.; Archer, T.; Gobbe, M. Stability of LASIK in corneas with forme fruste or suspect keratoconus, where keratoconus was excluded by epithelial thickness mapping. American Academy of Ophthalmology Annual Meeting; 9 Nov 2008; Atlanta, GA.
57. thoe Schwartzenberg GWS, Pavlin CJ. Occult wound leak diagnosed by ultrasound biomicroscopy in patients with postoperative hypotony. J Cataract Refract Surg 2001;27:549–54. [PubMed: 11311622]

58. Machemer HF, Roters F. Ultrasound biomicroscopy of chronic hypotony after cataract extraction. J Cataract Refract Surg 2001;27:327–9. [PubMed: 11226802]
59. Inazumi K, Gentile RC, Lee KY-C, et al. Ultrasound biomicroscopic diagnosis of cyclitic membranes. Am J Ophthalmol 2001;131:446–50. [PubMed: 11292407]
60. Gentile RC, Pavlin CJ, Liebmann JM, et al. Diagnosis of traumatic cyclodialysis by ultrasound biomicroscopy. Ophthalmic Surg Lasers 1996;27:97–105. [PubMed: 8640444]
61. Berinstein DM, Gentile RC, Sidoti PA, et al. Ultrasound biomicroscopy in anterior ocular trauma. Ophthalmic Surg Lasers 1997;28:201–7. [PubMed: 9076793]
62. Ozdal MPC, Mansour M, Deschenes J. Ultrasound biomicroscopic evaluation of the traumatized eyes. Eye 2003;17:467–72. [PubMed: 12802344]
63. Oliveira C, Liebmann JM, Dodick JM, et al. Identification of retained nucleus fragment in the posterior chamber using ultrasound biomicroscopy. Am J Ophthalmol 2006;141:964–6. [PubMed: 16678523]
64. Pavlin CJ, Harasiewicz K, Eng P, Foster FS. Ultrasound biomicroscopic analysis of haptic position in late-onset, recurrent hyphema after posterior chamber lens implantation. J Cataract Refract Surg 1994;20:182–5. [PubMed: 8201571]
65. Rondeau MJ, Barcsay G, Silverman RH, et al. Very high frequency ultrasound biometry of the anterior and posterior chamber diameter. J Refract Surg 2004;20:454–64. [PubMed: 15523957]
66. Oh J, Shin HH, Kim JH, et al. Direct measurement of the ciliary sulcus diameter by 35-megahertz ultrasound biomicroscopy. Ophthalmology 2007;114:1685–8. [PubMed: 17822974]
67. Werner L, Izak AM, Pandey SK, et al. Correlation between different measurements within the eye relative to phakic intraocular lens implantation. J Cataract Refract Surg 2004;30:1982–8. [PubMed: 15342066]
68. Demirci H, Nelson CC. Ultrasound biomicroscopy of the upper eyelid structures in normal eyelids. Ophthal Plastic Reconstr Surg 2007;23:122–5.
69. Bajaj MS, Aalok L, Gupta V, et al. Ultrasound biomicroscopic appearances of eyelid lesions at 50-MHz. J Clin Ultrasound 2007;35:424–9. [PubMed: 17551943]
70. Kikkawa DO, Ochabski R, Weinreb RN. Ultrasound biomicroscopy of eyelid lesions. Ophthalmologica 2003;217:20–3. [PubMed: 12566868]
71. Dai S, Kraft SP, Smith DR, Buncic JR. Ultrasound biomicroscopy in strabismus reoperations. J Am Assoc Ped Ophthalmol Strab 2006;10:202–5.
72. Nolan W. Anterior segment imaging: ultrasound biomicroscopy and anterior segment optical coherence tomography. Curr Opin Ophthalmol 2008;19:115–21. [PubMed: 18301284]
73. Silverman RH, Ketterling JA, Coleman DJ. High-frequency ultrasonic imaging of the anterior segment using an annular array transducer. Ophthalmology 2007;114:816–22. [PubMed: 17141314]
74. Hu CH, Xu XC, Cannata JM, et al. Development of a real-time, high-frequency ultrasound digital beam-former for high-frequency linear array transducers. IEEE Trans Ultrason Ferroelectr Freq Control 2006;53:317–23. [PubMed: 16529106]
75. Mamou J, Ketterling JA, Silverman RH. Chirp coded excitation imaging with a high-frequency ultrasound annular array. IEEE Trans Ultrason Ferroelectr Freq Control 2008;55:508–13. [PubMed: 18334358]
76. Duck FA. Nonlinear acoustics in diagnostic ultrasound. Ultra Med Biol 2002;28:1–18.
77. Kim HH, Cannata J, Liu R, et al. 20-MHz/40-MHz Dual element transducers for high frequency harmonic imaging. IEEE Trans Ultrason Ferroelectr Freq Control. (in press).
78. Silverman RH, Kruse D, Coleman DJ, Ferrara KW. High-resolution ultrasonic imaging of blood-flow in the anterior segment of the eye. Invest Ophthalmol Vis Sci 1999;40:1373–81. [PubMed: 10359319]
79. Cucevic V, Brown AS, Foster FS. Thermal assessment of 40-MHz pulses Doppler ultrasound in human eye. Ultra Med Biol 2005;31:565–73.
80. Zhou Q, Xu X, Gottlieb EJ, et al. PMN-PT single crystal, high-frequency ultrasonic needle transducers for pulsed-wave Doppler application. IEEE Trans Ultrason Ferroelectr Freq Control 2007;54:668–75. [PubMed: 17375836]
81. Lyshchik A, Fleischer AC, Huamani J, et al. Molecular imaging of vascular endothelial growth factor receptor 2 expression using targeted contrast-enhanced high-frequency sonography. J Ultra Med 2007;26:1575–86.

82. Huang C, Liu B, Brezinski ME. Ultrasound-enhanced optical coherence tomography: improved penetration and resolution. J Opt Soc Am 2008:938–46.

83. Nightingale KR, Palmeri ML, Nightingale RW, Trahey GE. On the feasibility of remote palpation using acoustic radiation force. J Acoust Soc Am 2001;110:625–34. [PubMed: 11508987]

84. Xu M, Wang LV. Photoacoustic imaging in biomedicine. Rev Sci Instrum 2006;77:041101-1-21.

85. Zhang HF, Maslov K, Stoica G, Wang LV. Functional photoacoustic microscopy for high-resolution and noninvasive in vivo imaging. Nat Biotechnol 2006;24:848–51. [PubMed: 16823374]

Figure 1.
UBM image (Cornell prototype system) of normal anterior segment image acquired using arc-scan.

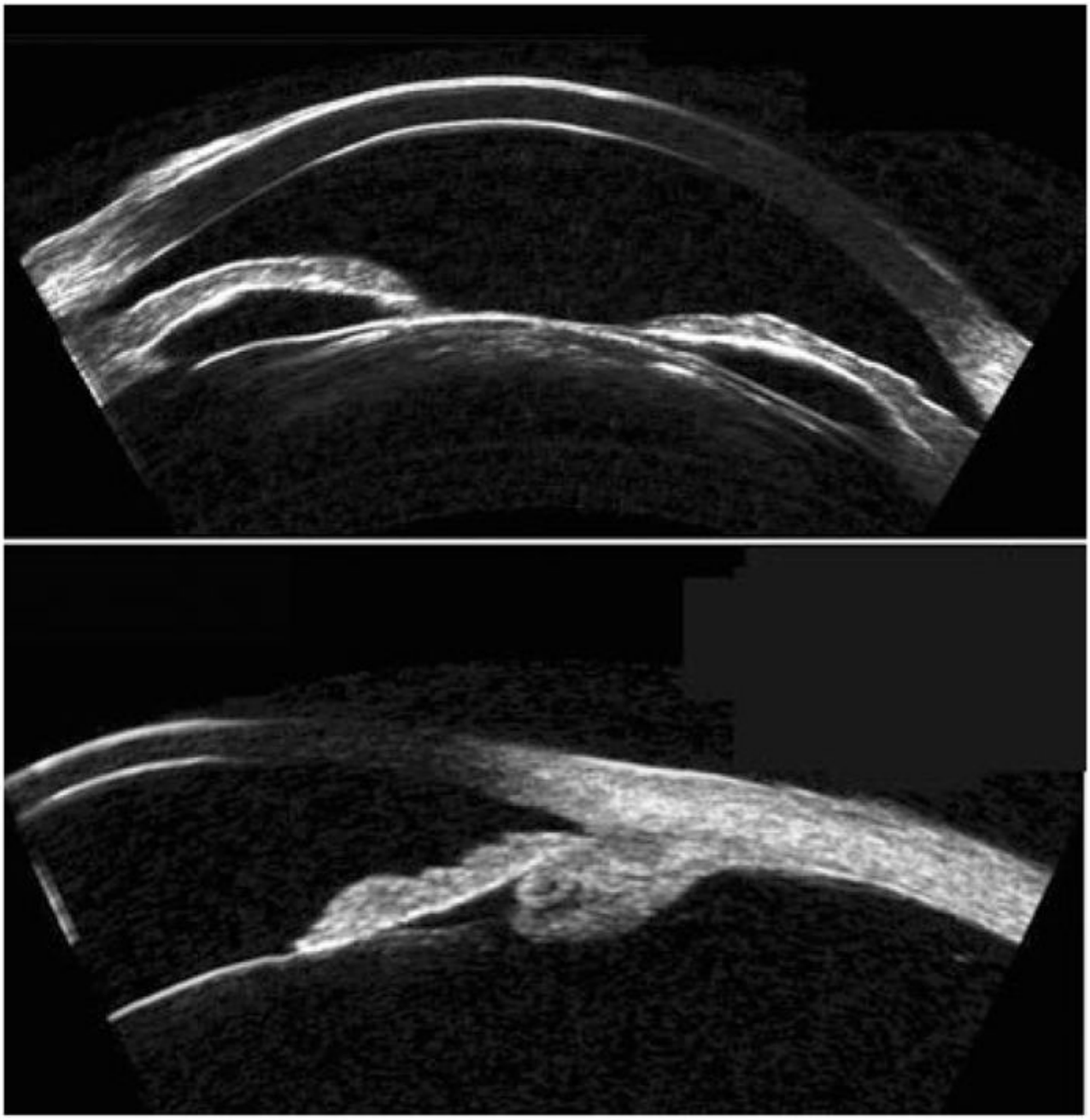

Figure 2.
Top: Pupillary block is characterized by forward bowing of iris due to pressure differential between anterior and posterior chambers. Note cataract. Bottom: Plateau iris syndrome. Note characteristic forward position of ciliary processes and blunting of sulcus. Images acquired with Cornell arc-scan prototype system.

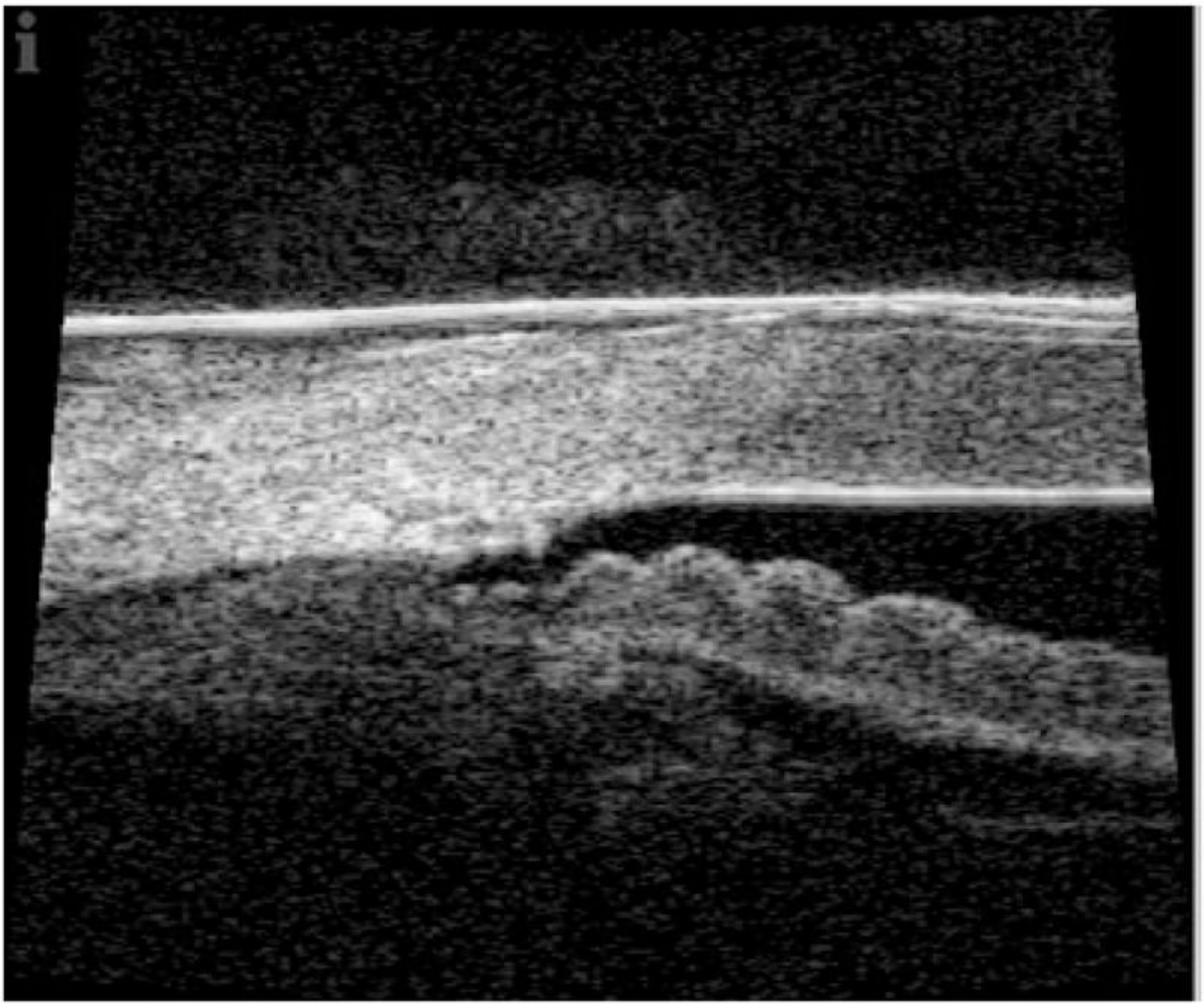

Figure 3.
80 MHz image of angle structures temporally in eye 18 months post canaloplasty. Images acquired with IScience IUl-traSound system. (Image courtesy of Dr Hulgar Bull and Dr Kurt von Wolff.)

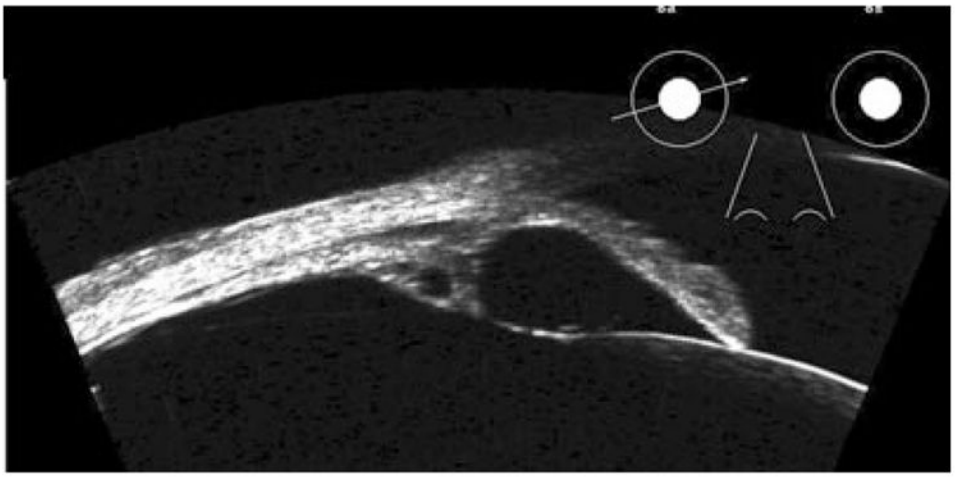

Figure 4.
Retroiridal cysts may cause bowing of overlying iris, as shown here. Also note secondary cyst in ciliary body. Images acquired with Cornell arc-scan prototype system.

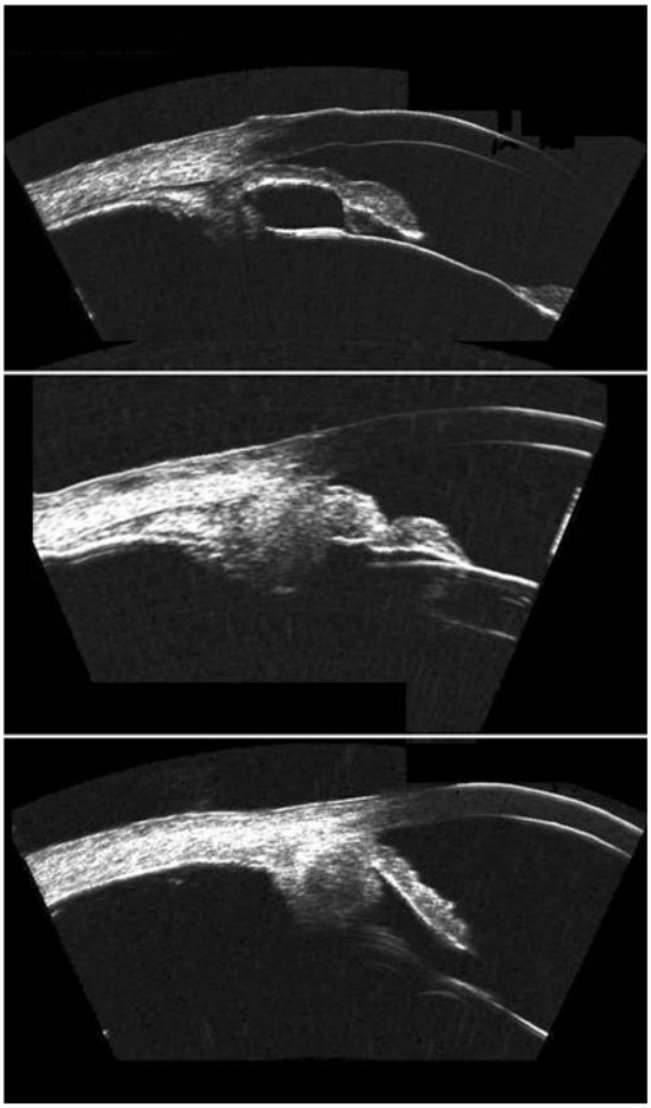

Figure 5.
Top: Malignant melanoma of the iris at pupil margin. Middle: Pigmented lesion of the iris in the region of the angle demonstrating extension to the ciliary body. Bottom: Ciliary body melanoma. Note 'cystic' component, which may be attributable to regions within the melanoma differing in pigmentation and/or cell type. Images acquired with Cornell prototype arc-scanner.

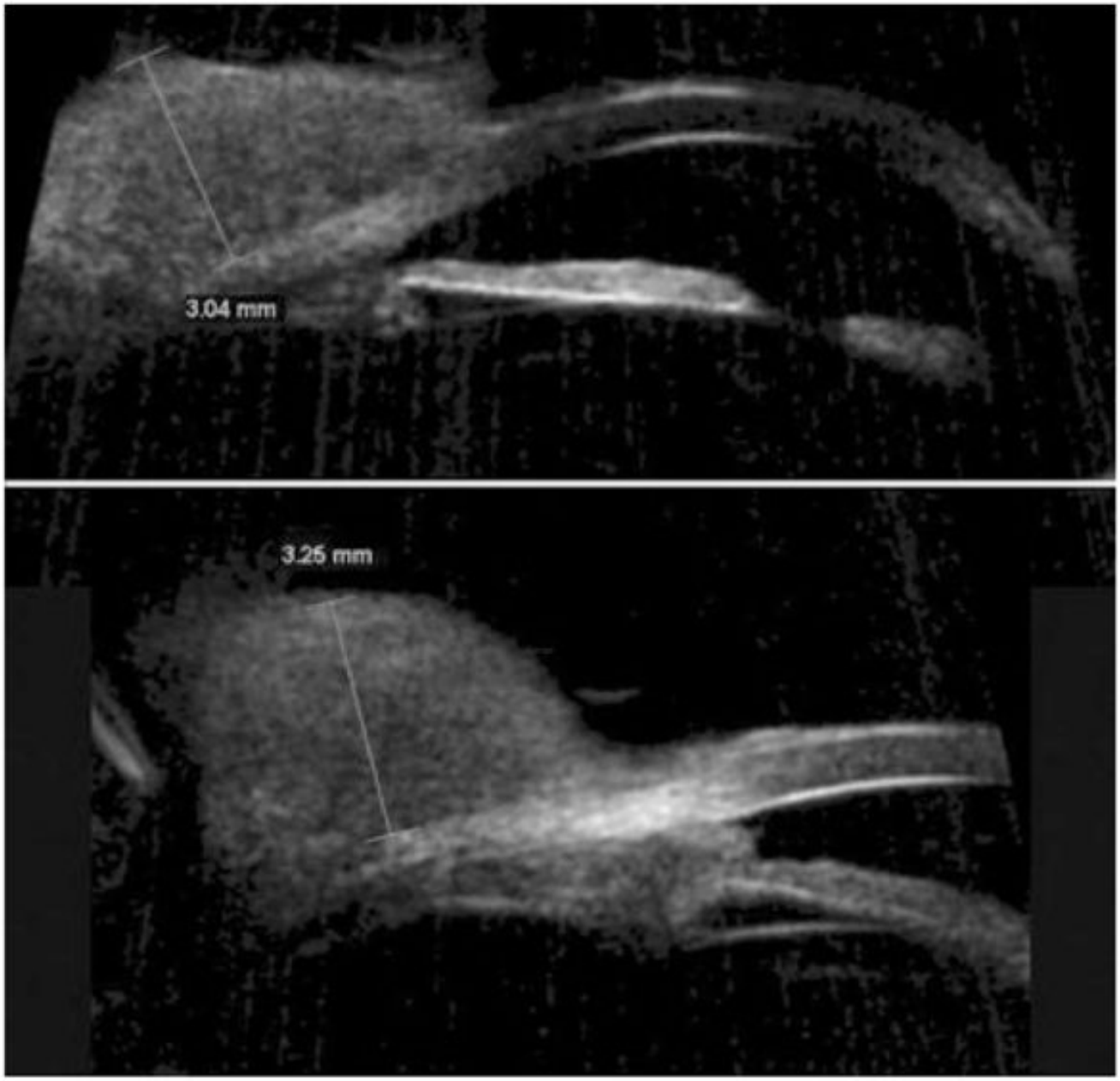

Figure 6.
Conjunctival spindle cell carcinoma. Top: Radial scan demonstrating a solid homogeneous conjunctival lesion, height: 3.04 mm. Bottom: Scan of adjacent area demonstrates extension into iridocorneal angle in anterior chamber. Scans performed with 50 MHz Sonomed VUMAX system. (Image courtesy of Norma Allemann, MD.)

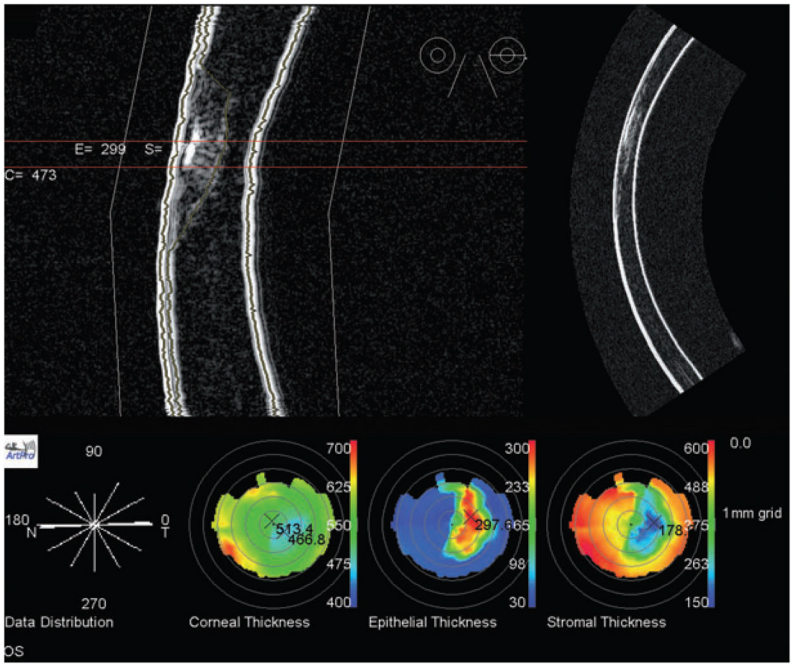

Figure 7.

Top: Artemis-2 B-mode images of corneal scar in horizontal plane in stretched rectilinear format (left) and geometrically corrected format (right). Bottom: Pachymetric maps formed from a series of scan meridians demonstrate scar location and extent. Corneal thickness map shows that the thinnest part of the cornea is displaced inferotemporally from the central cornea (thickness 514 μm) to the position of the scar, consistent with corneal thinning at the scar. The scar extends to a depth of approximately 300 mm, with an overall corneal thickness of about 470 mm at the scar position.

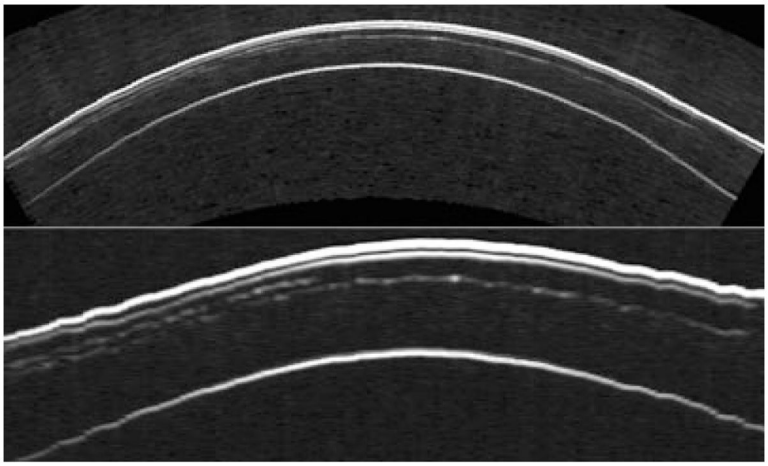

Figure 8.

An incomplete flap occurred during the primary LASIK treatment of this eye because of the patient's squeezing during the Hansatome microkeratome pass. Two months later, the patient was scanned using the Artemis-1 and the maximum flap thickness was measured to be 176 μm. The patient was then retreated using the VisuMax femtosecond laser (Carl Zeiss Meditec, Jena, Germany) with a programmed flap thickness of 190 μm so that the second flap would be deeper than the first flap. The images, top in geometrically correct format, bottom in stretched rectilinear format, show the cornea in the horizontal meridian after the second procedure. Both the initial, incomplete Hansatome flap and the complete VisuMax flap interfaces can be clearly seen. (Image courtesy of Dan Z. Reinstein, MD MA[Cantab] FRCSC.) LASIK, laser *in situ* keratomileusis.

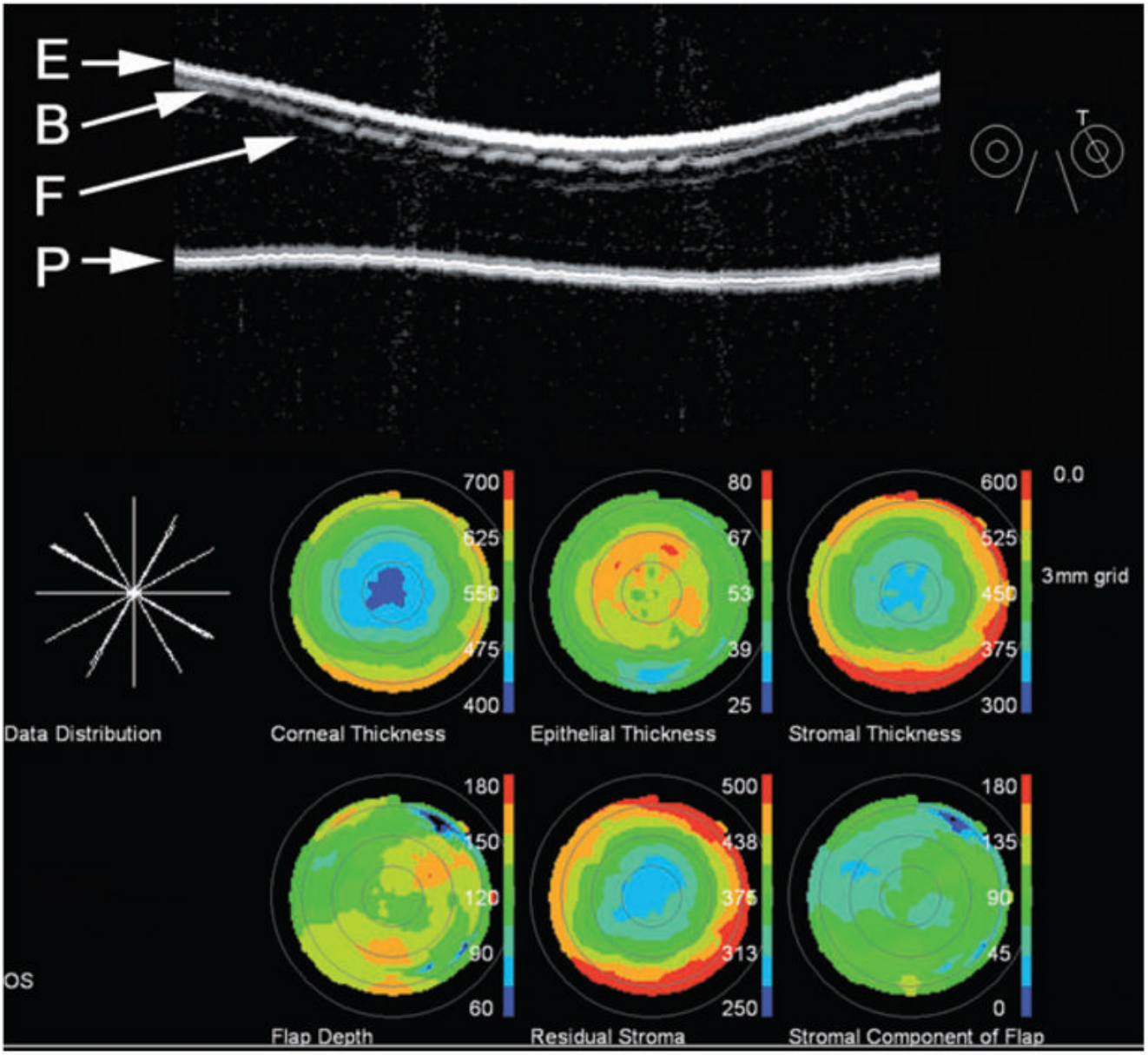

Figure 9.

Top: Artemis-2 scan of post-LASIK cornea shown in 'stretched' rectilinear format. The flap is readily seen. Also notable are interruptions in the Bowman's membrane interface, suggestive of microfolds. Bottom: The pachymetric maps were reconstructed from measurements of the epithelial surface (E), Bowman's membrane (B), the flap (F) and the posterior corneal surface (P) along scans at each of six clock-hours. Note irregular flap depth and thickening of the epithelium over the flap. LASIK, laser *in situ* keratomileusis.

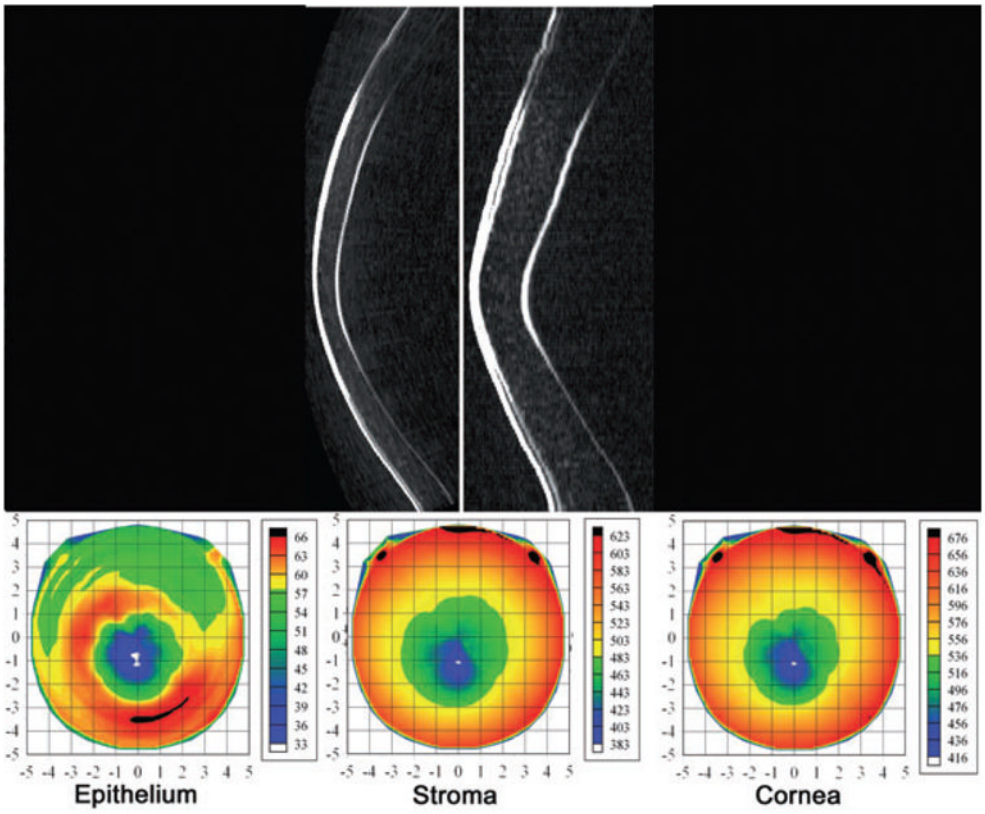

Figure 10.
Top: Geometrically and non-geometrically corrected vertical Artemis B-scan images of a patient with advanced keratoconus. Bottom: Pachymetric maps of the epithelium, stroma and cornea. Note area of epithelial thinning with a surround of epithelial thickening centred slightly inferior to the central cornea. This pattern occurs as the epithelium remodels in response to forward bulging of the underlying stroma. (Image courtesy of Dan Z. Reinstein, MD MA [Cantab] FRCSC.)

Figure 11.
Hyphaema following bungee-cord injury, with organized blood inferiorly and more diffuse blood suspended in the anterior chamber. Scans performed with Sonomed UBM. (Image courtesy of Roxana Ursea, MD.)

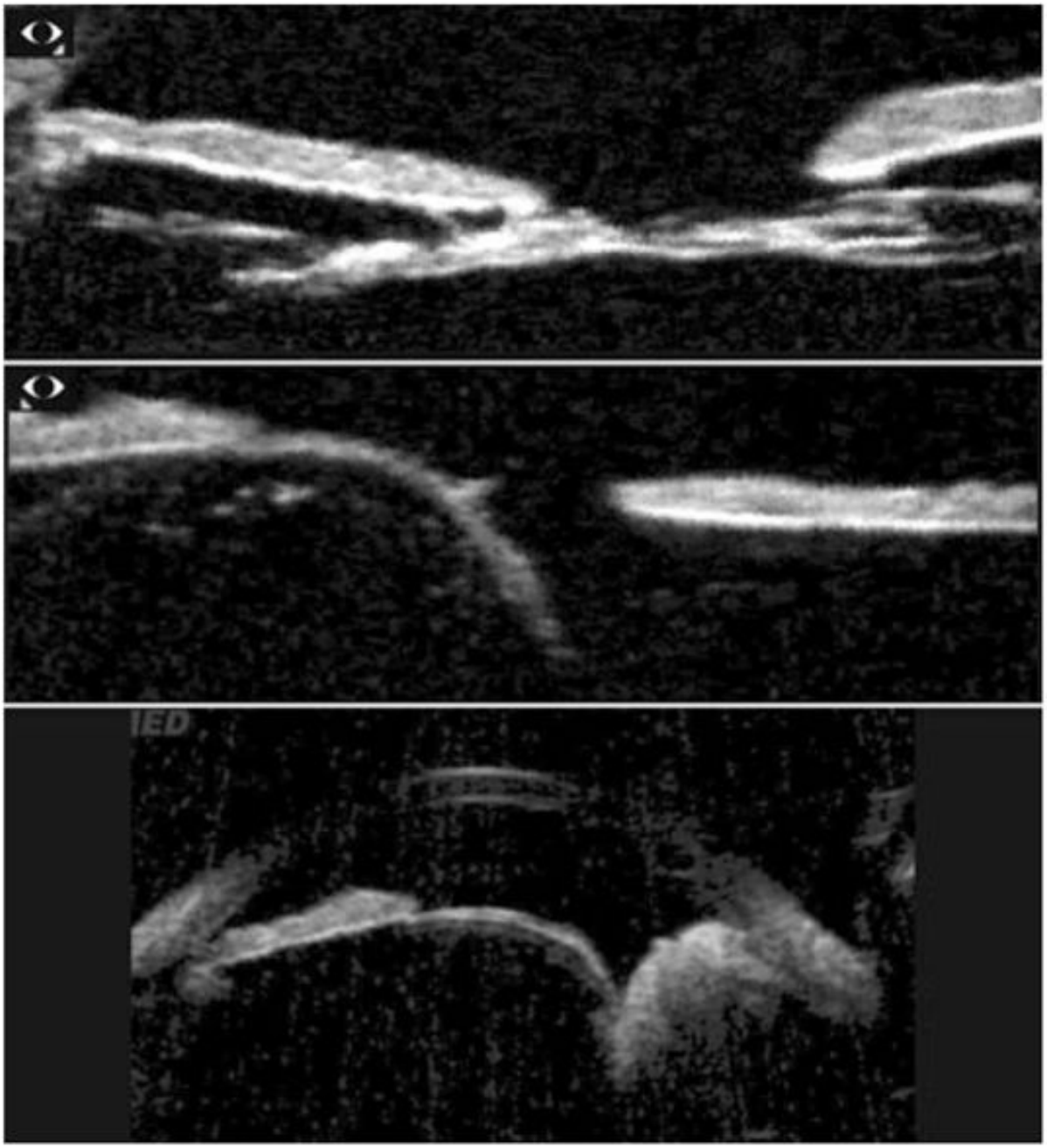

Figure 12.
Top: Congenital cataract demonstrates reduced lens thickness. Centre: Lens subluxation in Marfans' syndrome. Bottom: Lens subluxation secondary to ciliary body tumour. Scans performed with Sonomed VUMAX. (Images courtesy of Norma Allemann, MD.)

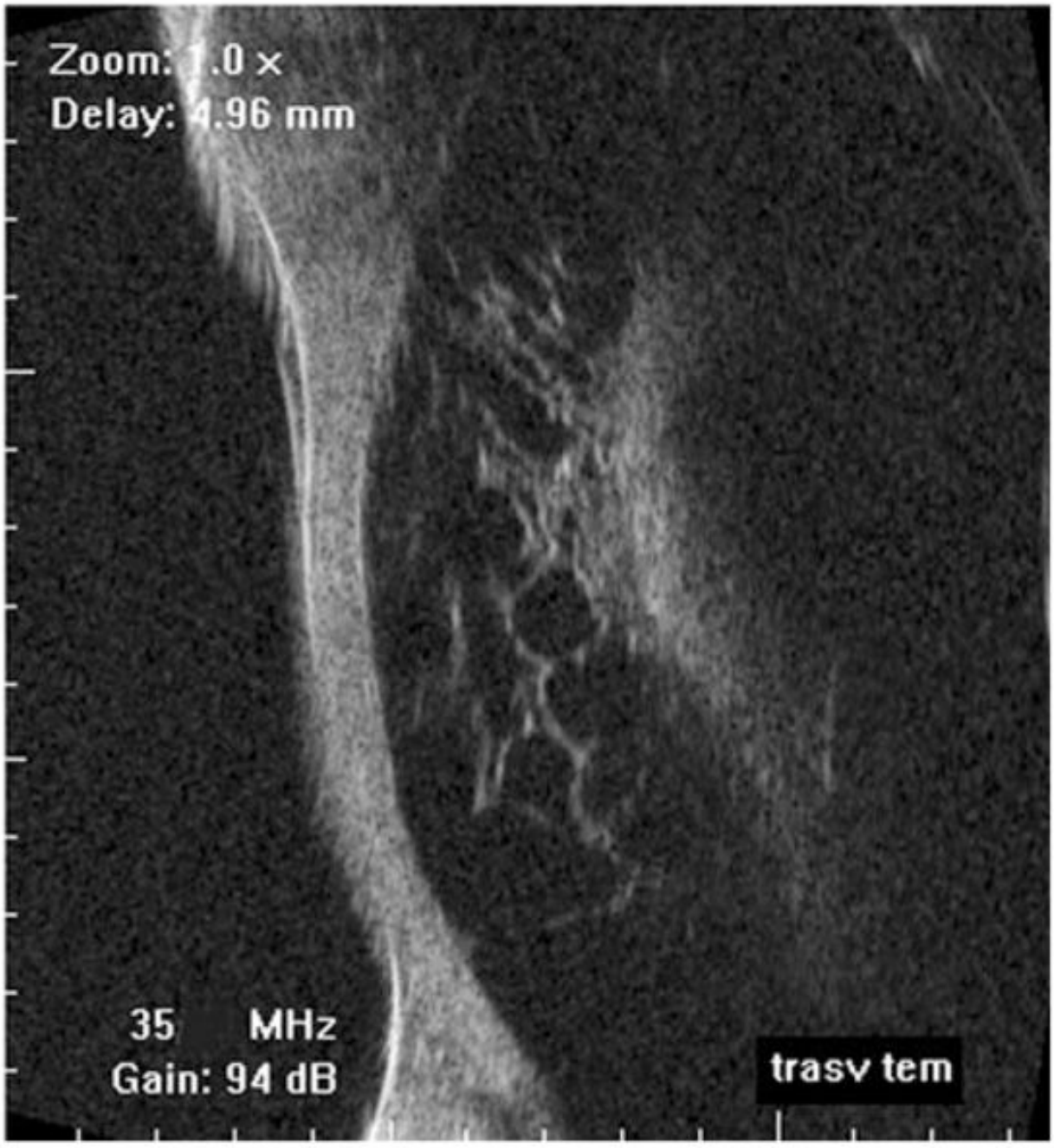

Figure 13.
Spontaneous ciliary body detachment. Scan performed by contact exam using probe cap on Optikon HiScan. (Image courtesy of Vincenzina Mazzeo, MD.)

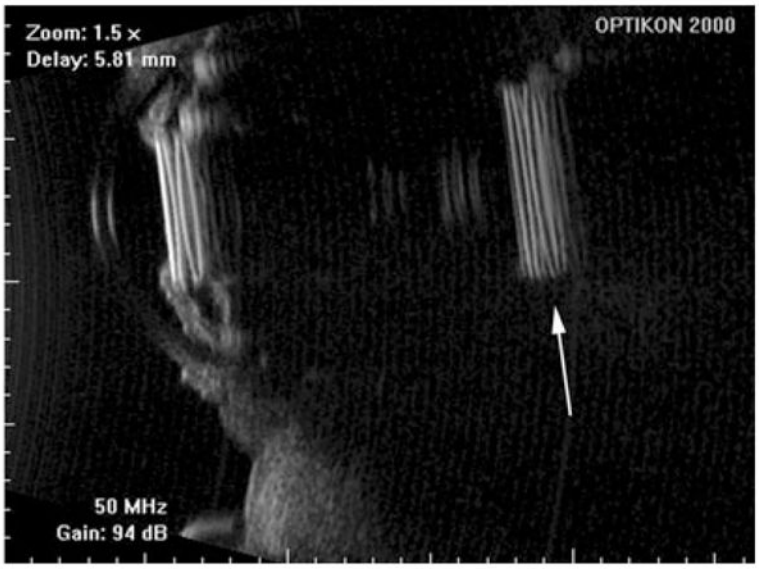

Figure 14.
Piggyback lens implants. Note reduplication artifact (arrow) resulting from multiple reflections of highly specular and reflective implants. Scans performed with Optikon HiScan. (Image courtesy of Vincenzina Mazzeo, MD.)

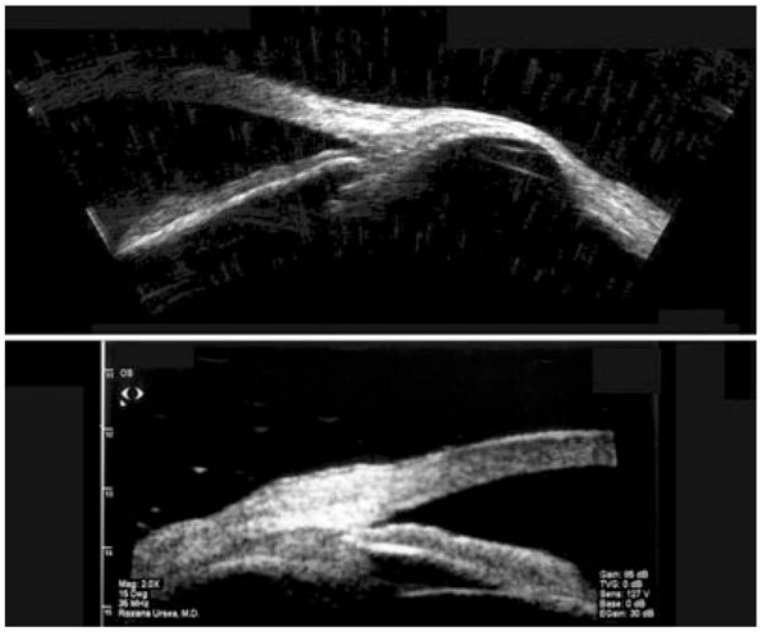

Figure 15.
Top: Scleromalacia 6 years following ruptured globe. Image acquired using Cornell prototype scanner. Bottom: Thickened sclera in localized anterior uveitis, demonstrated with Sonomed UBM. (Image courtesy of Roxana Ursea, MD.)

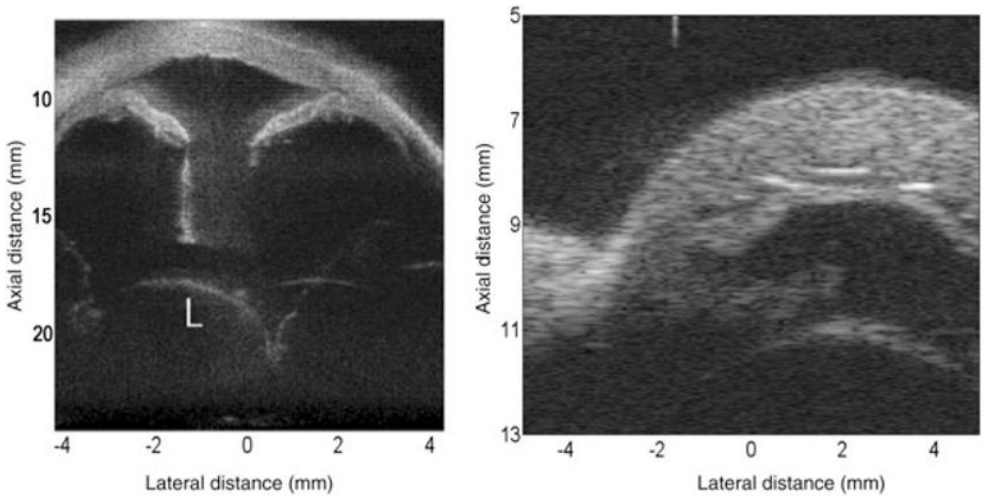

Figure 16.

Left: Image of anterior of *ex vivo* human eye made with 5-element 40 MHz annular array with chirp excitation. The combination of pulse encoding and synthetic focusing provides increased sensitivity and depth-of-field, enabling visualization of the dislocated lens. (Image courtesy of Jeffrey Ketterling, PhD and Jonathan Mamou, PhD.) Right: Anterior segment of *ex vivo* rabbit eye obtained with 64-element 30 MHz linear array using bipolar pulses and synthetic focusing. (Image courtesy of K. Kirk Shung, PhD, Jonathan Cannata, PhD and Xu Xiao-Chen, PhD.)

Table 1

Comparative properties of typical 10 MHz ophthalmic B-scanner and UBM system

Characteristic	Conventional B-Scanner	UBM
Frequency (MHz)	10	50
Aperture (mm)	10	6
Focal length (mm)	30	12
F-ratio	3	2
Axial resolution (μm)	150	30
Lateral resolution (μm)	450	60
Depth of field (mm)	9.6	0.85
Attenuation in water (dB/mm)	0.02	0.55